Low-Temperature Phases of Rubidium Silver Iodide: Crystal Structures and Dynamics of the Mobile Silver Ions†

Klaus Funke,*,‡ Radha D. Banhatti,‡ Dirk Wilmer,‡ Robert Dinnebier,§ Andrew Fitch,|| and Martin Jansen§

University of Münster, Institute of Physical Chemistry and Sonderforschungsbereich 458, Corrensstrasse 30/36, 48149 Münster, Germany, Max Planck Institute for Solid State Research, Heisenbergstrasse 1, 70569 Stuttgart, Germany, and European Synchrotron Radiation Facility, 6 rue Jules Horowitz, BP 220, 38043 Grenoble CEDEX, France

Received: August 25, 2005

Recently, broad-band conductivity spectra have been taken in the low-temperature γ-phase of the archetypal fast ion conductor $RbAg_4I_5$. Attempts to reproduce the experimental data in a simple model calculation have led to the conclusion that strictly localized displacive movements of interacting ionic charge carriers should play an important role in the low-temperature phase. However, with no detailed structural study of γ-$RbAg_4I_5$ available, the relevant processes could not be identified within the crystal structure. This state of affairs has triggered the present investigation of the structures of all three phases of rubidium silver iodide. Powder diffraction data of $RbAg_4I_5$ have been collected at the high-resolution powder diffractometer at ID31 at the European Synchrotron Radiation Facility (ESRF). The structure of the γ-phase has been solved by successive Rietveld refinements in combination with difference Fourier analyses. The same structural principle is found to prevail in all three phases, interconnected distorted RbI_6 octahedra forming a three-dimensional framework, which undergoes only displacive structural changes during the $\alpha-\beta$ and $\beta-\gamma$ phase transitions. With decreasing temperature, the disorder in the silver sublattice is found to decrease, and a clustering of the disordered silver ions is found to develop. In the γ-phase, "pockets" containing partially occupied silver sites have been identified, and it is suggested that the localized displacive motion detected by conductivity spectroscopy is performed by the silver ions located within these pockets.

I. Introduction

Rubidium silver iodide, $RbAg_4I_5$, is an archetypal member of the class of optimized crystalline silver ion conductors with structurally disordered silver sublattices.[1−3]

The high-temperature phase, traditionally called α-$RbAg_4I_5$, is cubic ($P4_132$). Upon cooling, it transforms into the rhombohedral ($R32$) β-phase at 209 K (second-order phase transition) and into the trigonal γ-phase at 122 K (first-order phase transition).[4] Remarkably, a detailed study of the crystal structure of the γ-phase does not exist.

In α-$RbAg_4I_5$, both the crystal structure and the dynamics of the mobile silver ions are rather well understood.[1,5,6] A popular way of describing the structurally disordered silver sublattice of α-$RbAg_4I_5$ is in terms of zigzag-shaped channels which are formed by alternating tetrahedral silver sites, Ag(1) and Ag(2). The channels are directed along the ⟨100⟩ directions and serve as intersecting diffusion pathways for the silver ions. Per unit cell, the cubic structure provides 24 Ag(1) sites and 24 Ag(2) sites for 16 silver ions. The rhombohedral β-phase bears close structural similarity to α-$RbAg_4I_5$.

Broad-band conductivity spectra extending up to infrared frequencies have been taken in all three phases of $RbAg_4I_5$.[7] Immediately below the phonon frequency regime, slow vibrational movements of the silver ions have been detected around 500 GHz. At millimeter-wave frequencies and below, the conductivity is, however, determined by the hopping dynamics of the mobile silver ions.

In Figure 1, we recall experimental frequency-dependent conductivities of rubidium silver iodide.[7] Vibrational contributions—which always vary as frequency squared on their low-frequency flank—have been carefully removed. In the figure, the symbols represent the conductivity isotherms thus obtained at different temperatures in the phases α, β, and γ.

The solid lines in Figure 1 are model spectra derived from the MIGRATION concept.[8,9] The meaning of the acronym is MIsmatch Generated Relaxation for the Accommodation and Transport of IONs. The MIGRATION concept and the previous CMR[6] (concept of mismatch and relaxation) are identical, apart from their respective properties in the low-frequency limiting behavior, which are irrelevant in the present context. Excellent agreement between experimental conductivity spectra and MIGRATION-type model spectra has been established for many ion-conducting materials with disordered structures including crystals, glasses, and undercooled melts.[6,10]

At this point, the physical basis of the MIGRATION concept, see Figure 2, is briefly outlined. In the model, each mobile ion is surrounded by its mobile neighbors, which create a "cage-effect potential" for it. Figure 2 shows a situation shortly after a hop of an ion from the site on the left to the site on the right. By this "initial" hop, mismatch is created, the actual position of the ion being different from the position where it is "expected" by its neighbors. In the following, the system tries

* Corresponding author. E-mail: k.funke@uni-muenster.de.
† Part of the special issue "Jürgen Troe Festschrift".
‡ University of Münster.
§ Max Planck Institute for Solid State Research.
|| European Synchrotron Radiation Facility.

10.1021/jp054807v CCC: $33.50
Published on Web 12/07/2005

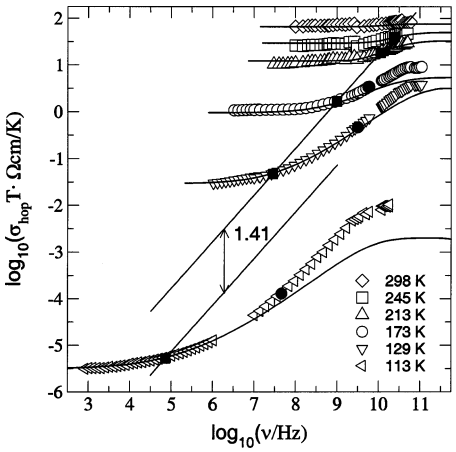

Figure 1. Conductivity isotherms of crystalline rubidium silver iodide, $RbAg_4I_5$, in its α, β, and γ phases. The vibrational contribution to the conductivity has been removed. Solid lines result from the MIGRATION concept. Full boxes and full circles mark the onset frequencies, $\nu_0 = \omega_0/2\pi$ and the frequencies corresponding to the elementary hopping rates, $\nu_1 = \Gamma_0/2\pi$, respectively. In both β and γ phases, the onset points constitute straight lines with slope one.

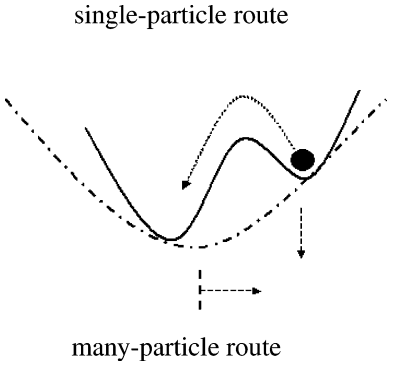

Figure 2. The two competing ways of mismatch relaxation in the framework of the MIGRATION concept: single-particle route vs many-particle route.

to reduce the mismatch, which is possible along either one of two competing routes. One is the "single-particle" route, with the ion hopping backward; the other is the "many-particle route" with the neighbors rearranging (see Figure 2). The mismatch-generated relaxation process occurring along the many-particle route finally leads to an accommodation of the ion at its new site. In this case, an elementary step of translational transport of the ion has been successfully completed. This model concept has been expressed in a set of simple rate equations. Eventually, linear response theory is used to derive model conductivity spectra from functions obtained from the rate equations.[11]

The problem to be tackled in this paper concerns the structure and the ion dynamics in the low-temperature phases of rubidium silver iodide, and it is directly related to the spectra presented in Figure 1. Evidently, the MIGRATION concept is able to describe the hopping dynamics of the silver ions very well in the α-phase, less well in the β-phase, and rather badly in the γ-phase. With decreasing temperature, we observe increasing differences between the experimental and the model spectra. These differences are restricted to the high-frequency parts of the spectra and, therefore, call for consideration of an additional fast process, which is not accounted for in the initial formulation of the MIGRATION concept.

This additional fast process has now been identified. The first step was made on the basis of the conductivity spectra, when the fast process in demand was explained in terms of activated hops that remain localized.[12] To reproduce the spectral shape of the fast conductivity component, which is of the NCL (nearly constant loss) type,[13,14] it was essential to consider (Coulomb) interactions between the ions involved in these localized movements. Inclusion of the NCL-type component was also found necessary to model the entire frequency-dependent spectra in glasses and salt-in-polymer systems.[15,16] Final evidence proving that localized ionic hopping within "pockets" or "islands" is, indeed, to be expected in the low-temperature phases of $RbAg_4I_5$ has now been obtained from new structural information, in particular on the γ-phase, see below. In fact, this is one of the rare examples where a structural property has been correctly deduced from the dynamics prior to its verification by actual structural investigations.

Another feature in Figure 1 that needs to be explained concerns the translational transport of the silver ions. At the $\beta-\gamma$ phase transition, we observe an interesting discontinuity in the scaling behavior, that is, the straight lines that mark the onset of the dispersion in phases β and γ are shifted with respect to each other by about 1.4 decades.[12]

In the following, we present the crystal structure of the γ-phase of crystalline rubidium silver iodide. Emphasis is put on the underlying structural principles. In light of these results, the questions posed by the spectra of Figure 1 are then revisited and answered in a consistent fashion.

II. Crystal Structure: Experimental Section

Powder diffraction data of $RbAg_4I_5$ were collected at the high-resolution powder diffractometer at ID31 at the European Synchrotron Radiation Facility (ESRF).

An Si(111)- reflection was used to select an X-ray energy of 30.99 keV. The size of the beam was adjusted to 2×0.6 mm^2 using slits. The wavelength was determined to be 0.40009(5) Å from a silicon standard. The sample of $RbAg_4I_5$ was contained in a 0.3-mm lithium borate glass capillary. The sample was rotated around θ in order to improve randomization of the crystallites. The diffracted beam was analyzed with a nine-crystal analyzer stage (nine Ge(111) crystals separated by 2° intervals) and detected with nine Na(Tl)I scintillation counters simultaneously. The incoming beam was monitored by an ion chamber for normalization of the decay of the primary beam. Scans of 15 min were taken at $T = 298$ K (α-phase), $T = 150$ K (β-phase), and $T = 90$ K (γ-phase) in continuous mode for 1 h each. They were later normalized and converted to step scan data for values of 2θ from 0.5° to 32.92°, in steps of 0.002°.

To ensure that the phase transformations were completed and to minimize the effect of decomposition, only identical scans were summed up at each temperature. For the low-temperature scans, a Cryostream 700 series cold-air blower manufactured by Oxford Cryosystems was used with a temperature stability of better than 1 K in the investigated temperature range. The low-temperature powder pattern of $RbAg_4I_5$ at 90 K is presented in Figure 3. The color of the sample was changing where it was hit by the beam, indicating some possible radiation damage. After some time, however, the sample seemed to recover, which is not usually the case where radiation damage occurs.

Data reduction of the low-temperature powder diffraction pattern of $RbAg_4I_5$ at $T = 90$ K was performed using the GUFI program.[17] Starting values for the lattice parameters of $RbAg_4I_5$ were taken from the paper by Geller.[5] According to the extinction rules, the most probable space group was $P3_121$, which could later be confirmed by Rietveld refinements.[18] The number of formula units per unit cell ($Z = 12$ for hexagonal axes) directly followed from volume increments. From the

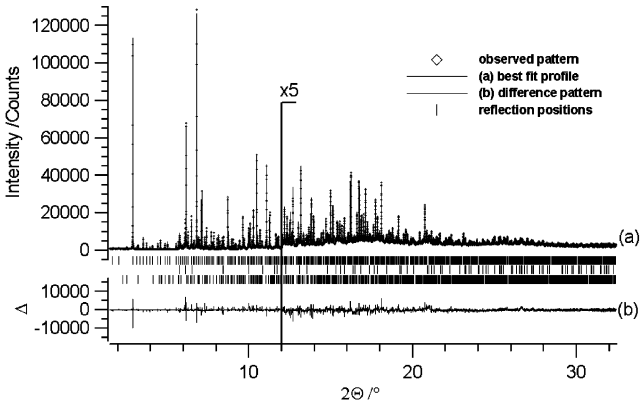

Figure 3. Scattered X-ray intensities for the low-temperature γ-phase of $RbAg_4I_5$ at $T = 90$ K as a function of diffraction angle 2θ. Shown are the observed pattern (diamonds), the best Rietveld-fit profile in $P3_121$ (line a), the difference curve between observed and calculated profile (line b), and the reflection markers (vertical bars). Rb_2AgI_3 and AgI are refined as additional phases. The wavelength was $\lambda = 0.40009(3)$ Å. The higher angle part starting at 12° 2θ is enlarged by a factor of 5.

literature it is known that during the 209 K $\alpha-\beta$ phase transition, the maximum shift which occurs in the framework buildup by rubidium and iodide ions is below 0.1 Å, while the silver ions move by a maximum of 0.3 Å.[5] It was thus expected that at least the framework remains stable also for the low temperature γ-phase, allowing the crystal structure to be solved by successive Rietveld refinements in combination with difference Fourier analysis.

The peak profiles and precise lattice parameters were determined by LeBail fits[19] using the program GSAS.[20] The background was modeled manually using GUFI. The peak profile was described by a pseudo-Voigt function[21] in combination with a special function that accounts for the asymmetry due to axial divergence.[22]

Two impurity phases, Rb_2AgI_3[23] and AgI, see, for example, ref 24, were detected and included in the refinement.

The shapes of the Bragg reflections of all three phases could be adequately described using only the size-dependent $1/\cos\theta$ term of a pure Lorentzian distribution, ruling out strain-related sample broadening. Atomic starting parameters for the Rietveld refinement were calculated from the β-phase in $R32$ using the program KPLOT.[25] The background and starting values for the peak profile were taken from the corresponding LeBail fit. An absorption correction for Debye−Scherrer geometry was applied, as well as a correction for anomalous scattering according to the KEK-tables.[26]

At the beginning of the refinement, all iodide and rubidium ions were kept fixed at their calculated positions. All silver ions were allowed to move within the unit cell, and sites were simultaneously allowed to change their occupancies. Strong damping factors were applied to the refined parameters. Those silver sites that refined to almost zero occupancy were removed, while those refining to an occupancy close to 1 were fixed at full occupancy. Consecutive difference Fourier cycles revealed possible positions for further silver ions, which were included in the refinement process.

At the time, when serious differences in the electron density could no longer be detected, all ions were slowly released with one overall temperature factor for each sort of them. As expected, the rubidium and iodide ions remained very close to their calculated positions. The refinement converged satisfactorily. Agreement factors (R-values) are listed in Table 1, the coordinates are given in Table 2, and a selection of intra- and intermolecular distances and angles is given in Table 3.

TABLE 1: Experimental Details of the Crystal Structure Determination of γ-$RbAg_4I_5$ at $T = 90$ K (Estimated standard deviations are in parentheses)

space group	$P3_121$ (Nr. 152)
unit cell dimensions	
a (Å)	15.8004(1)
c (Å)	19.3347(1)
unit cell volume (Å^3)	4180.26(6)
formula units in unit cell	12
calculated density (g/cm^3)	5.316
wavelength (Å)	0.40009(4)
data points	9000
range for data collection (°)	$2.0 \le 2\theta \le 20.0$
parameters	111
no. of reflections	1821
R-values	
R_F	10.2
$R_F{}^2$[a]	15.9
R_p[a]	11.72
R_{wp}[a]	16.32
χ^2	3.27

[a] Ref 20.

TABLE 2: Positional Parameters, Isotropic Displacement Parameters, and Fractional Occupancies of γ-$RbAg_4I_5$ at $T = 90$ K (Estimated standard deviations are in parentheses)

atom	Wy	x/a	y/b	z/c	u/Å^2	frac
RB(1)	3b	0.4313(18)	0.4313(18)	1/2	0.043(3)	1.0
RB(2)	6c	−0.0823(14)	−0.3317(12)	0.4910(9)	0.043(3)	1.0
RB(3)	3a	−0.2930(16)	−0.2930(16)	0	0.043(3)	1.0
I(1)	6c	0.3809(8)	0.1717(8)	0.4598(5)	0.026(1)	1.0
I(2)	6c	0.1508(8)	−0.1241(8)	0.4743(5)	0.026(1)	1.0
I(3)	6c	0.4444(9)	−0.0773(9)	0.4560(5)	0.026(1)	1.0
I(4)	6c	−0.0074(7)	−0.1364(8)	0.2712(5)	0.026(1)	1.0
I(5)	6c	0.4838(8)	−0.2032(8)	0.2822(6)	0.026(1)	1.0
I(6)	6c	0.5522(8)	0.3651(8)	0.2795(6)	0.026(1)	1.0
I(7)	6c	−0.1177(9)	0.5505(9)	0.3371(6)	0.026(1)	1.0
I(8)	3a	−0.2221(11)	0	1/3	0.026(1)	1.0
I(9)	3b	−0.1378(10)	−0.1378(10)	1/2	0.026(1)	1.0
I(10)	6c	0.4805(8)	−0.3146(8)	0.5038(6)	0.026(1)	1.0
I(11)	6c	−0.3223(8)	−0.3221(8)	0.6486(5)	0.026(1)	1.0
AG(1)	6c	0.5849(12)	0.2705(12)	0.4905(9)	0.013(1)	0.698
AG(2)	6c	0.3210(12)	−0.2688(13)	0.4864(8)	0.013(1)	0.712
AG(3)	6c	−0.4485(13)	−0.3839(15)	0.7797(9)	0.013(1)	0.69
AG(4)	6c	0.6453(8)	0.3600(9)	0.6252(6)	0.013(1)	1.0
AG(5)	6c	−0.0421(22)	−0.0744(21)	0.6255(13)	0.013(1)	0.399
AG(6)	6c	0.4697(15)	0.6264(15)	0.2594(10)	0.013(1)	0.6
AG(7)	6c	−0.2659(15)	0.5498(15)	0.2907(10)	0.013(1)	0.583
AG(8)	6c	−0.2026(8)	−0.1645(9)	0.2601(6)	0.013(1)	1.0
AG(9)	6c	0.0379(8)	−0.0623(8)	0.4117(5)	0.013(1)	1.0
AG(10)	6c	0.5727(12)	0.2997(12)	0.4085(8)	0.013(1)	0.704
AG(11)	6c	0.5315(14)	0.5187(14)	0.2685(9)	0.013(1)	0.625

TABLE 3: Selected Interatomic Distances (in Å) of γ-$RbAg_4I_5$ at $T = 90$ K (Estimated standard deviations are in parentheses)

Rb−I	3.38(2) ... 3.97(2)
Rb−Ag (min)	3.94(3)
I−Ag (min)	2.62(3)
Ag−Ag (disordered)	1.49(3) ... 2.35(4)
Ag−Ag (ordered)	min 2.57(3)

A quantitative Rietveld analysis proved that the sample investigated consisted of approximately 80% γ-$RbAg_4I_5$, 10% Rb_2AgI_3, and 10% AgI. The overall occupancy of the silver sites sums up to 4.01 per formula unit, verifying that all silver ions were located in the unit cell by the procedure described above.

Rietveld refinements for the α- and β-phases of $RbAg_4I_5$ confirmed the crystal structures from the literature.[1,5]

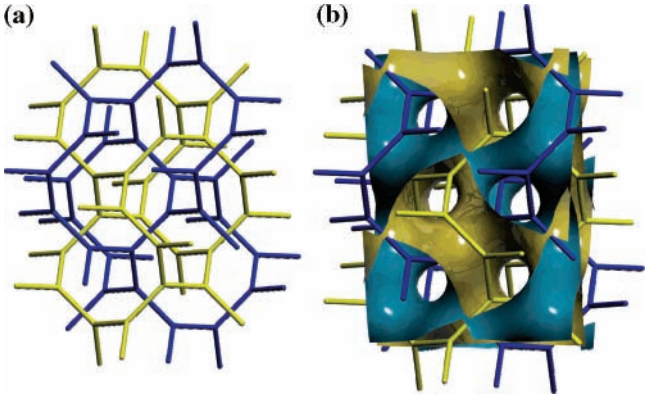

Figure 4. (a) The cubic (*Ia*-3*d*) 3-connected 10-gon net (10,3). The two interpenetrating nets are colored blue and yellow. (b) Cubic (10,3) nets of Figure 1 with isosurface.

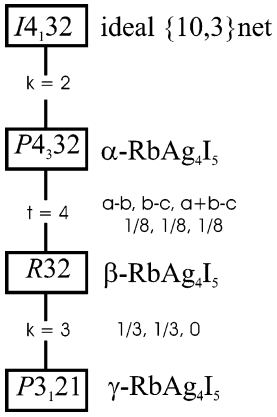

Figure 5. Group−subgroup relationships[29] relevant for $RbAg_4I_5$; t = translationengleich, k = klassengleich.[30]

III. Crystal Structure: Results and Discussion

As a characteristic feature, the crystal structure of $RbAg_4I_5$ can be separated in a virtually rigid part consisting of rubidium and iodide ions and the more-or-less disordered silver ions.

The rigid part is formed by distorted RbI_6 octahedra, which are interconnected by their 6 corners leading to $[RbI_3]_\infty$. This $[RbI_3]_\infty$ framework contains hexagonal channels, in which the two remaining iodide ions, which are not part of the $[RbI_3]_\infty$ scaffold, are located close to the walls of these channels.

The structure of the rigid $[RbI_3]_\infty$ network and the partial structure containing the dynamically disordered silver ions topologically correspond to two pairs of three-dimensional networks of the same generic symmetry and can be described by two interpenetrating 10,3 nets,[27,28] see Figure 4a.

The silver ions, a temperature-dependent fraction of which are disordered, occupy different positions within the channels of the $[RbI_3]_\infty$ framework, as will be discussed in more detail below. No unreasonably short contacts were found within the $[RbI_3]_\infty$ entity or between the silver ions and the atoms of the $[RbI_3]_\infty$ partial structure. By calculating and drawing the zero potential surfaces, one is able to generate a space divider separating the silver part from the $[RbI_3]_\infty$ part of the structure (Figure 4b).

During the phase transitions from cubic α-$RbAg_4I_5$ ($P4_132$) to rhombohedral β-$RbAg_4I_5$ ($R32$) to trigonal γ-$RbAg_4I_5$, the space group symmetry is significantly reduced. At the same time, however, only displacive structural changes are noticeable within the RbI_5-part of the structure. This offers the opportunity of displaying the structural relationships by a sequence of maximal group−subgroup relations, limiting the possible space groups for γ-$RbAg_4I_5$ to either $P321$ or $P3_121$. By applying the extinction rules and by preserving the interpenetrating (10,3)-nets, it turns out that the correct space group for the γ-phase is $P3_121$ and not $P321$ as suggested earlier.[5]

The group−subgroup relationships, starting from an ideal (10,3)-net are illustrated by a so-called Bärnighausen-tree,[29] see Figure 5. Amazingly, $Ag_4Mn_3O_8$, although a compound of quite different chemical nature and composition, shows the same general structural properties, including the identical sequence of phase transitions from cubic via rhombohedral to trigonal space groups.[31]

The overall topology of $RbAg_4I_5$ as described above is maintained in all three modifications (Figure 6). The most pronounced structural changes, including the phase transitions, occur within the silver partial structure. Two groups of silver ions can be identified. Those on sites with mutual distances greater than two times the ionic radius of octahedrally coordinated Ag^{1+} cations (2.52 Å) are regarded as ordered, while those on sites with mutual distances below 2.52 Å are identified as disordered. Although jumps of silver ions between well-separated sites are possible, disordered silver ions play the prominent role in explaining the high conductivity of $RbAg_4I_5$.

In the high-temperature α-phase of $RbAg_4I_5$, the silver ions are highly disordered, with short contacts existing between 90% of the available sites. Altogether, they form a three-dimensional arrangement (Figure 6a), thus explaining the high ionic conductivity of this phase.

With decreasing temperature, the disorder of the silver ions is found to decrease. In the medium-temperature β-phase, the silver ions are separated in two extended clusters, running along the trigonal *c*-axis. Now, uninterrupted short contacts only exist within but not between the clusters (Figure 6b), which suggests high ionic conductivity only in one preferred direction along the *c*-axis.

Finally, in the low-temperature γ-phase, only a few short contacts exist (Figure 6c). In contrast to the other two phases at higher temperatures, these short distances are restricted to isolated clusters [Ag(6)−Ag(11)−Ag(3)−Ag(7)], [Ag(2)−Ag(1)−Ag(10)−Ag(7)] which are not interconnected (Figure 7). The short distance of 2.1 Å between disordered Ag(5) and ordered Ag(9) suggests a further symmetry reduction to $P3_1$. This was, however, not pursued any further, due to instabilities in the three-phase refinement from powder diffraction data.

IV. Hopping Dynamics of the Silver Ions

Knowing the structures of all three phases of rubidium silver iodide, we may now correlate structural and dynamic data at different temperatures. Here, the low-temperature γ-phase is of particular interest. In the case of γ-$RbAg_4I_5$, it is important to distinguish silver-ion movements that remain localized and others that are "potentially translational" in the sense of the MIGRATION concept. The former are supposed to occur within the clusters of partially occupied sites that have been described above, while the latter require sites that are interconnected, forming passageways. Figure 8 serves for visualization, showing the "clusters" or "pockets" or "islands", each of them surrounded by corner-sharing distorted RbI_6 octahedra.

About 58% of the silver ions are located within these pockets, while the sites for the remaining 42% form a three-dimensional network extending throughout the crystal volume.

In Figure 9 we reconsider the conductivity spectrum taken at 113 K within the γ-phase, see Figure 1. The complete model

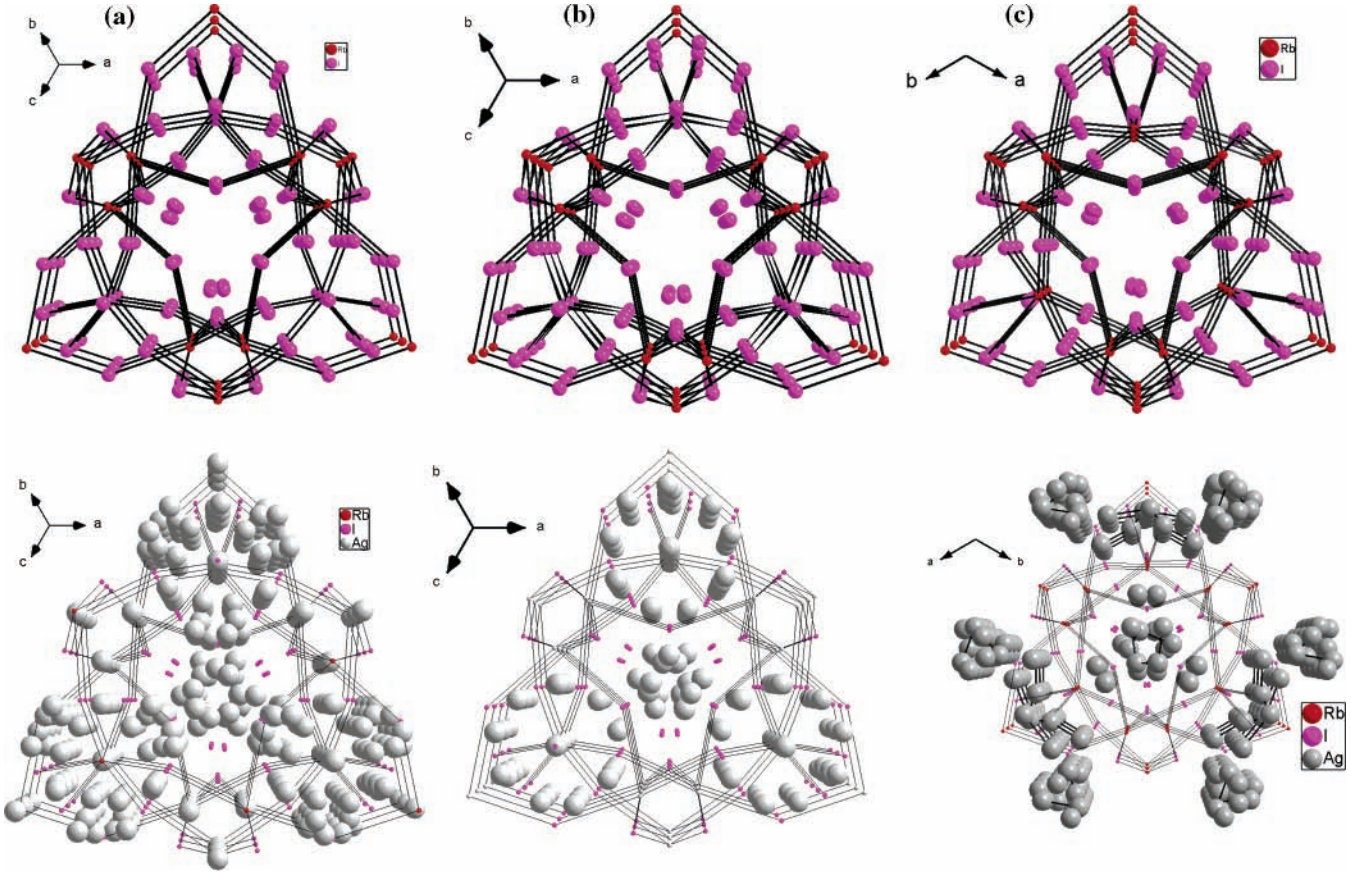

Figure 6. Projection of the crystal structures of α-$RbAg_4I_5$ at $T = 295$ K along [111] (a); β-$RbAg_4I_5$ at $T = 150$ K along [001] (b); γ-$RbAg_4I_5$ at $T = 90$ K along [001] (c). The upper part of the figure shows the $[RbI_3]_\infty$ framework plus intercalated iodide ions without silver ions, while the lower part shows the silver ions within a down-scaled framework.

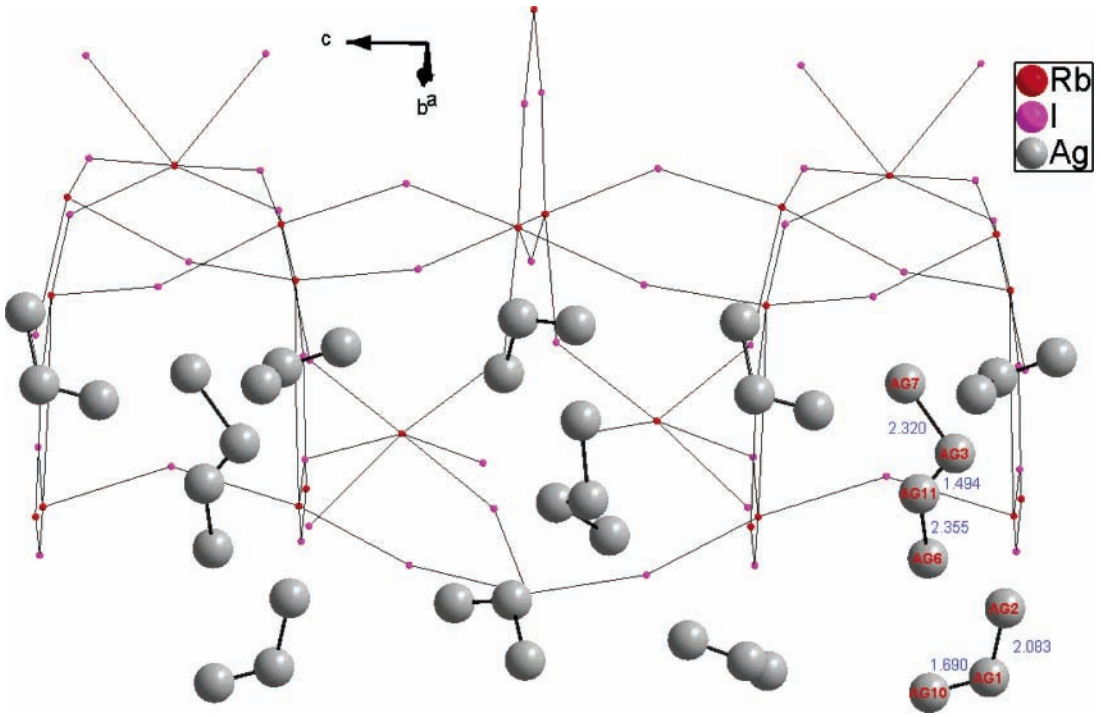

Figure 7. Projection of part of the crystal structures of γ-$RbAg_4I_5$ at $T = 90$ K along the trigonal channels showing only the isolated groups of disordered silver ions.

spectrum, which is also included in Figure 9, now consists of two components:

$$\sigma_{HOP}(\nu) = \sigma_{MIG}(\nu) + \sigma_{LOC}(\nu) \qquad (1)$$

One of them, $\sigma_{MIG}(\nu)$, is based on the original version of the MIGRATION concept and was already shown in Figure 1. The other, $\sigma_{LOC}(\nu)$, has been obtained from a modified version describing the localized hopping motion of interacting ionic charge carriers.[12] As the total model spectrum fits the experi-

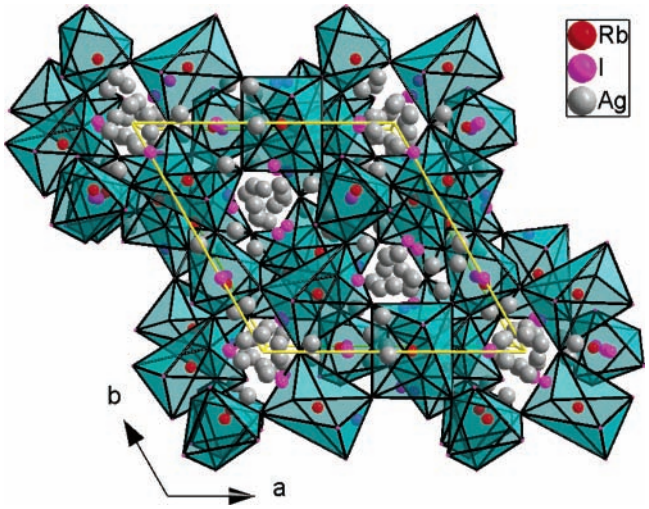

Figure 8. Perspective view of the crystal structure of γ-$RbAg_4I_5$ at $T = 90$ K along the c-axis. The strongly distorted RbI_6 octahedra are shown in light blue. Gray and purple spheres represent interstitial silver positions and nonbonded iodide ions, respectively.

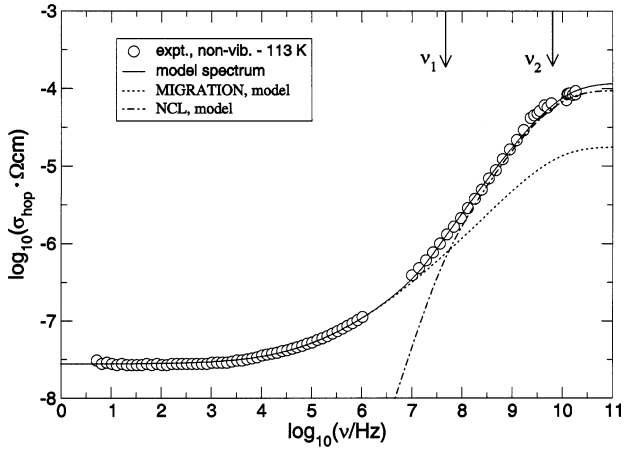

Figure 9. Nonvibrational conductivity spectrum of β-$RbAg_4I_5$ at 113 K (circles), along with a model spectrum (solid line). The spectrum is decomposed into its MIGRATION and NCL components. Arrows at frequencies ν_1 and ν_2 indicate the lower and upper limits of the regime where the conductivity varies linearly with frequency.

mental data very well, $\sigma_{LOC}(\nu)$ appears to be the conductivity component that was missing in Figure 1.

For reproducing the experimental data, best results are obtained with elementary hopping rates, Γ_0, that are identical for localized and potentially translational hops. The corresponding frequency, $\nu_1 = \Gamma_0/2\pi$, has been marked in Figure 9. It is interesting to note that a different behavior has been found in an ion-conducting glass, where the localized hops are much faster and thermally less activated than the potentially translational ones.[15]

The localized ionic hopping motion detected in the frequency-dependent conductivity is now identified with the displacive movements performed by disordered silver ions within their isolated pockets.

A simple argument may be used to estimate the number density of localized mobile charge carriers, n_{LOC}. Let $\sigma_{LOC,HF}$ denote the high-frequency limiting value of $\sigma_{LOC}(\nu)$ and x_{LOC} the elementary hopping distance for localized hops. Then, n_{LOC} may be obtained from

$$\sigma_{LOC,HF} = n_{LOC} \times \frac{(ex_{LOC})^2}{6k_BT} \times \Gamma_0 \qquad (2)$$

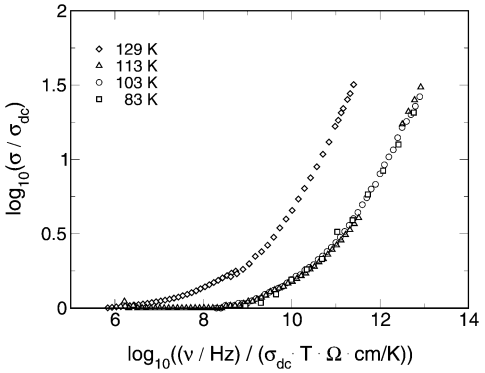

Figure 10. Scaled representations of conductivity isotherms of $RbAg_4I_5$ above and below the $\beta-\gamma$ phase transition. The figure proves that the Summerfield scaling is fulfilled within the γ-phase.

Depending on the choice of x_{LOC}, the value of n_{LOC} turns out to be one-fifth to one-quarter of the number density of all silver ions contained in the pockets. In view of the occupancies of the positions available for the silver ions, it appears reasonable to regard mobile vacancies rather than ions as carriers of effective charge within the pockets.

The dynamic information contained in the spectrum of Figure 9 may also be used for estimating the fraction of silver ions that are translationally mobile. The relevant expression is similar to eq 2, but now contains the respective parameters for MIGRATION-type hopping motion. As a result, we find slightly less than one mobile charge carrier of this kind within a unit cell. Again, these charge carriers have to be regarded as mobile vacancies carrying effective charge. The fraction of vacancies being so small, they have eluded detection in our structural investigation.

Interestingly, the fraction of vacancies on the three-dimensional silver network in γ-$RbAg_4I_5$ is found to be independent of temperature. This can be concluded from the scaled representation of Figure 10 where the low-frequency parts of three different γ-phase spectra have been superimposed.[12] A superposition of this kind, known as Summerfield scaling,[32] indicates that the transport mechanism (including the number of mobile charge carriers) is preserved as the temperature is changed.

Figure 10 also includes the low-frequency section of one β-phase spectrum. With respect to the γ-phase spectra, we observe an offset of about 1.4 decades on the normalized frequency scale. This corresponds to the discontinuity of 1.4 decades already noted in Figure 1. Because $1.4 \approx \log_{10}25$, we have

$$(n_{MIG} \cdot x_{MIG}^2)_\beta \approx 25(n_{MIG} \cdot x_{MIG}^2)_\gamma \qquad (3)$$

Here, n_{MIG} and x_{MIG} denote number densities and elementary hopping distances pertaining to the MIGRATION-type hopping motion. The ratio of the squares of the hopping distances in the two phases, $(x_{MIG}^2)_\gamma/(x_{MIG}^2)_\beta$, is clearly larger than one, probably close to two. As a γ-phase unit cell contains slightly less than one MIGRATION-type vacancy per 48 silver ions, eq 3 implies that, in the β-phase, the majority of the silver ions have to be regarded as disordered, contributing to macroscopic transport. Clearly, this is in agreement with the results of our structural analysis. However, there also seems to be some localized displacive motion in the β-phase, see Figure 1 and ref 12.

Finally, it is worth mentioning that the anisotropy of the translational silver-ion motion suggested by the structure of

β-$RbAg_4I_5$ cannot be detected in the conductivity spectra of Figure 1, the material used being polycrystalline.

V. Conclusion

Broad-band conductivity data of rubidium silver iodide in its low-temperature γ-phase have called for consideration of a localized hopping process of interacting silver ions in this material. Indeed, the experimental data are perfectly explained by superposition of two kinds of hopping motion, one of them being (potentially) translational in character, the other remaining localized. Although the localized hopping does not contribute to the DC conductivity, it dominates the conductivity at microwave frequencies, suggesting that many more silver ions are involved in the localized than in the translational kind of motion.

Until now, with detailed structural information on γ-$RbAg_4I_5$ not existing, the localized hopping processes could not be identified within the crystal structure. A sound basis for a better understanding is, however, provided by the present structural investigation, proving that isolated "clusters" or "pockets" of partially occupied silver sites are, indeed, available for localized displacive movements of the silver ions. Combining structural and dynamic data, it is now even possible to estimate the fractions of ionic charge carriers (vacancies rather than silver ions) that move within the pockets and on the three-dimensional network of interconnected silver sites.

Last, but not least, the evolution of the crystal structure of rubidium silver iodide as a function of temperature, comprising its phases α, β, and γ, turns out to be quite attractive from an aesthetic point of view. A common structural principle is found to prevail in all three phases, with rather small variations in the positions of the rubidium and iodide network ions entailing considerable changes in the silver sublattice, its disorder decreasing and clustering of disordered ions developing with decreasing temperature.

Acknowledgment. We thank Dr. A. Hannemann for the calculations with the KPLOT program.

References and Notes

(1) Geller, S. *Science* **1967**, *157*, 308.
(2) Bradley, J. N.; Greene, P. D. *Trans. Faraday Soc.* **1967**, *63*, 424.
(3) Owens, B. B.; Argue, G. R. *Science* **1967**, *157*, 308.
(4) Johnston, W. V.; Wiedersich, H.; Lindberg, G. W. *J. Chem. Phys.* **1969**, *51*, 3739.
(5) Geller, S. *Phys. Rev. B* **1976**, *14*, 4345.
(6) Funke, K.; Brückner, S.; Cramer, C.; Wilmer, D. *J. Non-Cryst. Solids* **2002**, *307*−*310*, 921.
(7) Ross, I. *Untersuchung der komplexen frequenzabhängigen ionischen Leitfähigkeit von RbAg4I5 unterhalb der Raumtemperatur*, Ph.D. Thesis, Münster, 2003.
(8) Funke, K.; Banhatti, R. D. *Mater. Res. Soc. Symp. Proc.* **2003**, *756*, 3.
(9) Funke, K.; Banhatti, R. D. *Solid State Ionics* **2004**, *169*, 1.
(10) Singh, P. *Fragility and the coupled-to-decoupled transition in supercooled molten calcium potassium nitrate studied by broad-band conductivity spectroscopy*, Ph.D. Thesis, Münster, 2005.
(11) Kubo, R. *J. Phys. Soc. Jpn.* **1957**, *12*, 570.
(12) Funke, K.; Banhatti, R. D.; Ross, I.; Wilmer, D. *Z. Phys. Chem.* **2003**, *217*, 1245.
(13) Lee, W. K.; Liu, J. F.; Nowick, A. S. *Phys. Rev. Lett.* **1991**, *67*, 1559.
(14) Lu, X.; Jain, H. *J. Phys. Chem. Solids* **1994**, *44*, 1433.
(15) Funke, K.; Banhatti, R. D.; Cramer, C. *Phys. Chem. Chem. Phys.* **2005**, *7*, 157.
(16) Pas, S. *A fundamental study of salt-in-polymer electrolytes*, Ph.D. Thesis, Münster, 2005.
(17) Dinnebier, R. E.; Finger, L. Z. *Kristallogr. Supplement Issue* **1998**, *15*, 148.
(18) Rietveld, H. M. *J. Appl. Crystallogr.* **1969**, *2*, 65.
(19) Le Bail, A.; Duroy, H.; Fourquet, J. L. *Mater. Res. Bull.* **1988**, *23*, 447.
(20) Larson, A. C.; von Dreele, R. B. *GSAS 1994, Version 2002*; Los Alamos National Laboratory Report LAUR 86-748, 2002.
(21) Thompson, P.; Cox, D. E.; Hastings, J. B. *J. Appl. Crystallogr.* **1987**, *20*, 79.
(22) Finger, L.; Cox, D. E.; Jephcoat, A. P. *J. Appl. Cryst.* **1994**, *27*, 892.
(23) Brown, I. D.; Howard-Lock, H. E.; Natarajan-Iyer, M. *Can. J. Chem.* **1977**, *55*, 1511.
(24) Berthold, H. J.; Kaese, P. M. *Z. Krist.* **1989**, *186*, 38.
(25) Hundt, R. *KPLOT: A Program for Plotting and Investigating of Crystal Structures*; University of Bonn, Germany, 1979.
(26) Sasaki, S. *Numerical Tables of Anomalous Scattering Factors Calculated by the Cromer and Liberman's Method*; Japanese National Laboratory for High Energy Physics KEK Report 88-14, 1989.
(27) Uniform 3-connected net, in which the shortest circuit including any pair of links from any point is a 10-gon with 3 edges meeting at each vertex.
(28) Wells, A. F. *Three-dimensional nets and polyhedra*; John Wiley & Sons: New York, London, Sydney, Toronto, 1977; ISBN 0-471-02151-2.
(29) Bärnighausen, H. *MATCH Commun. Math. Chem.* **1980**, *9*, 139.
(30) Hermann, C. *Z. Krist.* **1929**, *69*, 533.
(31) Ahlert, S.; Dinnebier, R. E.; Jansen, M. *Z. Anorg. Allg. Chem.* **2005**, *631*, 90.
(32) Summerfield, S. *Philos. Mag. B* **1985**, *52*, 9.